Submitted to ApJ
Preprint typeset using LaTeX style emulateapj v. 12/16/11

PROPAGATION AND STABILITY OF SUPERLUMINAL WAVES IN PULSAR WINDS

Iwona Mochol and John G. Kirk
Max-Planck-Institut für Kernphysik, Postfach 10 39 80, 69029 Heidelberg, Germany
Submitted to ApJ

ABSTRACT

Nonlinear electromagnetic waves with superluminal phase velocity can propagate in the winds around isolated pulsars, and around some pulsars in binary systems. Using a short-wavelength approximation, we find and analyze an integrable system of equations that govern their evolution in spherical geometry. A confined mode is identified that stagnates to finite pressure at large radius and can form a precursor to the termination shock. Using a simplified criterion, we find this mode is stable for most isolated pulsars, but may be unstable if the external pressure is high, such as in the pulsar wind nebulae in starburst galaxies and in W44. Pulsar winds in eccentric binary systems, such as PSR 1259-63, may go through phases with stable and unstable electromagnetic precursors, as well as phases in which the density is too high for these modes to propagate.

Keywords: plasmas – instabilities – waves – pulsars: general – stars: winds, outflows – ISM: supernova remnants

1. INTRODUCTION

Electromagnetic fields, modulated at the rotation frequency of the neutron star, form the energetically dominant component of pulsar winds. These flows are responsible for transporting the rotational energy lost by the star and depositing it in the surrounding pulsar wind nebula (PWN). As well as energy, they also convey the magnetic flux and the charged particles — most likely electrons and positrons — that are required to produce synchrotron radiation in the PWN (Rees & Gunn 1974).

An important property that sets pulsar winds apart from other stellar winds is their relatively low density. As a result, the fluctuations imposed by the rotation of the neutron star are able to propagate not only as MHD waves frozen in to the outflowing plasma, but, beyond a critical or cut-off radius r_c, also as large-amplitude electromagnetic modes of superluminal phase velocity (Asseo et al. 1975; Melatos & Melrose 1996). The location of the cut-off radius depends on the wave amplitude and on the relative strength of the phase-averaged fields and the fluctuating components, which, in turn, depend on the obliquity of the pulsar (i.e., the angle between its magnetic and rotation axes) and on latitude in the wind. For isolated pulsars it generally lies well inside the position where a termination shock can be expected (Arka & Kirk 2012), so that superluminal waves may play an important role in the outer parts of the wind and also in the termination shock itself. In particular, since they may carry the entire wind luminosity and are notoriously unstable (Max 1973; Drake et al. 1974; Asseo et al. 1980; Lee & Lerche 1980), they could provide the key to resolving the well-known "σ-problem".

This term is used to describe the lack of a convincing mechanism for converting Poynting flux into particle-carried energy flux. Poynting flux dominates the wind at launch, but is thought to be a small fraction of the energy budget outside the termination shock. Recent work (Porth et al. 2012) suggests that MHD instabilities in the shocked wind may, as proposed by Begelman (1998), be able to reduce σ (the ratio of Poynting flux to kinetic-energy flux) from a starting value of a few just outside the shock, to the value suggested by observation, which is $\sim 10^{-3}$ for the Crab Nebula (Kennel & Coroniti 1984b).

However, the mechanism underlying the transition from $\sigma \gg 1$ near the pulsar to $\sigma \sim 1$ at the termination shock remains controversial. Most work on this problem has concentrated on the damping of MHD like wave-modes either in the wind (Lyubarsky & Kirk 2001; Kirk & Skjæraasen 2003; Lyubarsky 2010) or at the termination shock itself, where current sheets carried into the shock are compressed, giving rise to dissipation by driven reconnection. (Lyubarsky 2003; Lyubarsky & Liverts 2008; Pétri & Lyubarsky 2007). In this scenario, particle acceleration is primarily associated with the dynamics of the reconnection region (Sironi & Spitkovsky 2011).

However, it has recently emerged that the termination shock structure may be very different in the region where superluminal modes can propagate. In this case, the mechanism of dissipation is closely connected with the parametric instabilities of these modes, rather than with driven reconnection (Amano & Kirk 2013). The associated particle acceleration mechanisms have not yet been investigated in detail, but it is suggested that the first order Fermi process may be much more prominent when superluminal waves are present, than in the case of dissipation by reconnection.

This question is central to the study of PWN, and especially their high energy (TeV) emission. Current models adopt ad hoc assumptions concerning the injection of accelerated particles at the termination shock which take no account of the role of the surrounding medium in determining the shock location and structure. In order to establish a predictive theory of pulsar winds, it is, therefore, fundamentally important to identify which PWN are likely to sustain shocks mediated by superluminal modes, and which are not, and to classify important properties such as the stability or instability of these modes at the position of the shock. These are the questions we address. Our approach builds on the work of

iwona.mochol@mpi-hd.mpg.de, john.kirk@mpi-hd.mpg.de

Arka & Kirk (2012), who found the shape of the cut-off surface $r = r_c$ for both linearly and circularly polarized waves of arbitrary amplitude, including, for the former, a non-zero value of the phase-averaged magnetic field. Here, we develop a perturbation method to determine how a superluminal mode launched outside the cut-off surface will evolve as it propagates radially outwards, searching for those regions of the wind in which such a packet remains relatively stable, and those in which it can be expected to thermalize rapidly.

In section 2 we recall the description of nonlinear superluminal plane waves in a two-fluid electron-positron plasma, and summarize the literature concerning their stability properties. Radially propagating waves in spherical geometry are treated in in section 3. First, the short-wavelength perturbation theory is developed and is shown to result in an integrable system of equations for the radial evolution of wave packets, consisting of the conservation laws of particles and energy, supplemented by an analogue of the entropy equation. Restricting, for simplicity, the treatment to circularly polarized modes, it is shown that two kinds of wavepacket are possible — freely expanding modes, which ultimately turn into vacuum waves, and confined modes, which stagnate at finite pressure, and can be identified as extended precursors of the termination shock. Section 3.4 discusses the confined modes and shows that two distinct regions exist in which they are relatively stable. One of these is relevant for pulsar winds in high pressure environments, such as the high-pressure wind of a companion star, the other is relevant for isolated pulsars in low-pressure surroundings, such as supernova ejecta. Analytical constraints are given on the values of pulsar period, surrounding pressure and mass-loading parameter μ that determine whether or not a pulsar wind has the potential to generate a stable superluminal precursor at its termination shock. In section 4 we discuss the significance and limitations of our results and their implications for PWN around isolated pulsars and in gamma-ray binaries. Finally, a brief summary of our main results is presented in section 5.

2. LARGE-AMPLITUDE PLANE WAVES

2.1. *Basic properties*

The simplest system able to describe superluminal modes is that of two cold charged fluids. It has been analyzed in detail by Clemmow (1974a, 1977). In the pulsar case, we are concerned with cold electron and positron fluids and, in particular, with electromagnetic modes in which the displacement current is non-zero in all frames of reference.

In the outer parts of a pulsar wind, the radial component of the magnetic field is very small, and will be neglected in the following. In this case, radially propagating electromagnetic waves have only transverse fields, but the fluid velocities can have a component in the direction of propagation. The waves are characterized by a superluminal phase speed $\beta_{\rm phase} > 1$ and a subluminal group speed $\beta_{\rm w} = 1/\beta_{\rm phase}$ and will henceforth be called simply "superluminal" modes. The electron and positron fluids have the same proper number density n, and move with the same velocity $p_\parallel/\gamma$ (in units of c) in the direction of wave motion. But the transverse velocity of the positrons $\vec{p}_\perp/\gamma$ is antiparallel to that of the electrons. (Here, γ is the Lorentz factor of the fluids, and $p_\parallel$ and $\vec{p}_\perp$ are components of the dimensionless four-velocity of the positron fluid). This generates a transverse conduction current. In the homogeneous or "H-frame", in which the group speed vanishes, the fluid and field variables are space-independent, and the conduction current exactly balances the displacement current. In general, $p_\parallel/\gamma$ differs from the wave group speed $\beta_{\rm w}$, implying a non-vanishing flux of particles in the H-frame.

The governing equations have been presented elsewhere (in Arka & Kirk 2012, for example), and are reproduced in Appendix A. The nonlinear solutions take their simplest form in the H-frame, where the phase variable (A1) is purely temporal. Circularly polarized modes are monochromatic (i.e., depend sinusoidally on phase) and have phase-independent $p_\parallel$. The phase-averaged fields vanish. Linearly polarized modes, on the other hand, have a "saw-tooth" dependence of $p_\parallel$ on phase, and may also carry a non-zero phase-averaged transverse magnetic field component perpendicular to the oscillating electric field.

Although the analytical treatment of linearly polarized modes is significantly more cumbersome, their dispersion curves, at least for vanishing phase-averaged magnetic field, are very similar to those of circularly polarized modes (Arka & Kirk 2012). Consequently, we restrict much of the following discussion to circularly polarized modes.

2.2. *Stability*

In unmagnetized plasmas, strong electromagnetic waves are subject to parametric instabilities. These are induced by longitudinal density fluctuations which can couple to the transverse electromagnetic side-band modes and cause backscattering, filamentation, or absorption of the driver (Max 1973; Drake et al. 1974). The growth rates can be as high as the wave frequency. The stability of self-consistent waves was first investigated in a nonrelativistic electron-ion plasma (Max & Perkins 1972; Max 1973). This work was extended to the relativistic case for electron-positron plasmas by Romeiras (1978) and Lee & Lerche (1978). In all cases only perturbations that propagate in the direction of driver's motion were discussed, and the dispersion relations were obtained by linearization. In general, it was found that both short- and long-wavelength perturbations are unstable. Finite-temperature effects can be expected to suppress the instabilities at short wavelengths, although, to our knowledge, a complete analysis is lacking. Long wavelength perturbations, on the other hand, are stable if the particle flux through the wave in the H-frame is sufficiently large. A simple criterion is given by Lee & Lerche (1978). Denoting quantities measured in the H-frame by a prime, they find stability when

$$S \equiv p_\parallel'^2 - 2\gamma' p_\perp + p_\perp^2 \; > \; 0 \; . \tag{1}$$

Numerical studies of Romeiras (1978) and the PIC simulations of Skjæraasen et al. (2005) confirm the stabilizing effect of relativistic streaming. Although no precise test of it has been undertaken, we nevertheless adopt (1) in the following as the stability criterion for circularly polarized modes, noting that for linearly polarized modes the presence of a phase-averaged transverse component

of the magnetic field has an additional stabilizing effect (Asseo et al. 1980).

2.3. *Electromagnetic Hugoniot curve*

Plane waves in this model can be characterized by the phase-averaged values of their particle flux density J, energy flux per particle μ, and parallel (i.e., in the propagation direction) momentum flux per particle ν. In a local analysis, waves in a radial pulsar wind can also be considered plane. A radial wind occupying a total solid angle $\Omega_{\rm s}$ is characterized by an energy flux L and a flux of electrons and positrons of $\dot{N}$, in terms of which the parameters μ and J are

$$\mu = L/\left(\dot{N}mc^2\right) \ , \tag{2}$$

$$J = \dot{N}/\left(\Omega_{\rm s} r^2\right) \ . \tag{3}$$

The momentum flux is connected with the magnetization parameter σ. In a cold, striped wind, it is (Kirk 2010)

$$\nu \approx \mu - \frac{\sigma}{2\mu} + \frac{\sigma^4}{8\mu^3} \tag{4}$$

(for $\mu \gg 1$ and $\sigma \lesssim \mu^{2/3}$) and is independent of radius, provided there is no dissipation. It is related to the ram pressure P (the (r,r) component of the stress-energy tensor) by

$$P = \frac{\nu}{\mu}\left(\frac{L}{\Omega_{\rm s} r^2 c}\right) \ . \tag{5}$$

Observations of the Crab Nebula suggest (e.g., Bucciantini et al. 2011)

$$L = 5\times 10^{38}\ {\rm erg\ s^{-1}} \ , \tag{6}$$

$$\dot{N} = 10^{40}\ {\rm s^{-1}} \ , \tag{7}$$

so that $\mu \approx 10^4$. Close to the star, a magnetically dominated wind is expected to accelerate rapidly until mildly super(magneto)sonic (Kirk et al. 2009) implying $\sigma \lesssim \mu^{2/3}$, so that $\nu \approx \mu$. For nonlinear waves, the wave group speed depends not only on the frequency, but also on other wave properties, such as the amplitude. Thus, in order to plot a dispersion curve, giving, for example the group speed as a function of frequency, additional constraints are needed. Choosing μ and ν to be constant along such a curve transforms it into the electromagnetic equivalent of a Hugoniot curve: it then specifies all the (plane) waves of a given frequency that can be launched in a pulsar wind characterized by the same values of μ and ν (Arka & Kirk 2012).

3. SPHERICAL WAVES

3.1. *Short-wavelength approximation*

The radial evolution of spherical nonlinear waves at distances from the origin large compared to the wavelength can be treated using standard perturbation techniques (Asseo et al. 1984; Kirk & Mochol 2011a,b). These lead straightforwardly to equations that express conservation of the phase-averaged particle and radial energy fluxes (Appendix A)

$$\frac{1}{r^2}\frac{\partial}{\partial r}\left(r^2\left\langle 2np_\parallel\right\rangle\right) = 0 \ , \tag{8}$$

$$\frac{1}{r^2}\frac{\partial}{\partial r}\left(r^2\left\langle 2np_\parallel\gamma\right\rangle + \frac{r^2\beta_{\rm w}\left\langle |E|^2\right\rangle}{4\pi mc^2}\right) = 0 \ . \tag{9}$$

However, the divergence of the (r,r) component of the stress-energy tensor does not yield a conservation law directly:

$$\frac{1}{r^2}\frac{\partial}{\partial r}\left(r^2\left\langle 2np_\parallel^2\right\rangle + \frac{r^2\left(1+\beta_{\rm w}^2\right)\left\langle |E|^2\right\rangle}{8\pi mc^2}\right) = \frac{\left\langle np_\perp^2\right\rangle}{r} \tag{10}$$

Nevertheless, as we show in the Appendix B, an integral of motion can be found by constructing the electrodynamic equivalent of the hydrodynamic entropy equation, essentially by subtracting $\beta_{\rm w}$ times the energy equation (9) from the momentum equation (10). This integral can be found more directly by considering the adiabatic invariants of the zeroth-order plane wave.[1] In both the lab. (pulsar) frame and the H-frame, the charge density of the wave vanishes, and both the current and the electric field are entirely transverse. This means that the electrostatic potential A^0 vanishes when the Coulomb gauge is chosen. It is then a trivial matter to construct an adiabatic invariant Φ of the motion of an individual fluid particle by integrating over one period of oscillation the zeroth component of the canonical momentum P^μ:

$$\begin{aligned}\Phi &= \oint {\rm d}t\, P^0 \\ &= \oint {\rm d}t\, \left(mc\gamma + eA^0/c\right) \\ &= 2\pi mc\left\langle\gamma\right\rangle/\omega\end{aligned} \tag{11}$$

where ω is the angular wave frequency in the lab. frame. In our case, ω equals the (constant) angular velocity of the pulsar, so that the invariance of Φ in a slowly expanding (or contracting) flow implies

$$\frac{\partial}{\partial r}\left\langle\gamma\right\rangle = 0 \ . \tag{12}$$

In addition, to these equations, Ampère's law provides a connection between the electric field and the fluid momentum:

$$\frac{\partial \vec{E}}{\partial t} = -mc\omega_{\rm p}^2\gamma_{\rm w}^2\vec{p}_\perp/e \ , \tag{13}$$

where $\gamma_{\rm w} = \left(1-\beta_{\rm w}^2\right)^{-1/2}$ is the Lorentz factor associated with the wave group speed, and $\omega_{\rm p} = \left(8\pi ne^2/m\right)^{1/2}$ is the proper plasma frequency.

3.2. *Circular polarization*

For simplicity, we now restrict the treatment to circular polarization, the corresponding expressions for linear polarization are given in Appendix C.

[1] We are indebted to an anonymous referee for suggesting this approach.

To close the system, a non-linear dispersion relation is required. For circular polarization, in which the variables n, γ, $|E|^2$, $|p_\perp|^2$, and $p_\parallel$ are all independent of phase, this is

$$\begin{aligned}\omega^2 &= \omega_{\rm p}^2 + c^2k^2 \\ &= \gamma_{\rm w}^2\omega_{\rm p}^2 \end{aligned} \tag{14}$$

and equation (13) reduces to

$$\frac{e^2|E|^2}{m^2c^2\omega^2} = |p_\perp|^2 \ . \tag{15}$$

Equations (8) and (9) can be integrated and combined with (14) and (15) to give

$$J = r^2 2np_\parallel \ , \tag{16}$$

$$\mu = \gamma + \frac{\gamma_{\rm w}^2\beta_{\rm w}p_\perp^2}{p_\parallel} \ , \tag{17}$$

where J and μ are the constants of integration. Equation (17) simply expresses the conservation of energy, in which the first term is the particle energy flux and the second the Poynting flux (per particle, in each case). In a pulsar wind, both of these quantities, and also the particle flux J, are expected to be positive, corresponding to outward-going fluxes. Thus, the relevant parameter space is restricted to $p_\parallel \geq 0$, $\beta_{\rm w} \geq 0$, and $\gamma \leq \mu$, and the bounding line $\mu = \gamma$ corresponds to waves of vanishing amplitude, $p_\perp = 0$.

As a wave packet propagates, its frequency remains locked to that of the pulsar. This determines the radial dependence of the wave via the continuity equation (16) and the dispersion relation (14): $p_\parallel \propto \gamma_{\rm w}^2/r^2$. In terms of the normalized radius R defined in Arka & Kirk (2012, Eq. 31):

$$R = r(\Omega_{\rm s}L\omega^2/4\pi c\dot{N}^2e^2)^{1/2}, \tag{18}$$

this relation is

$$p_\parallel = \frac{\mu\gamma_{\rm w}^2}{R^2} \ . \tag{19}$$

(Note that the cut-off radius $r_{\rm c}$ lies very close to, but just outside, the point $R = 1$.)

Using $\gamma^2 = 1 + p_\parallel^2 + p_\perp^2$ to eliminate $p_\perp$ and equation (19) to eliminate $p_\parallel$, we rewrite the equation of conservation of energy flux per particle (17) as

$$\frac{\mu^2\beta_{\rm w}^2\gamma_{\rm w}^4}{R^4} + (\mu-\gamma)\frac{\mu\beta_{\rm w}}{R^2} - \beta_{\rm w}^2(\gamma^2-1) = 0 \ . \tag{20}$$

This equation determines the radial dependence of the group speed of the wave $\beta_{\rm w}$, because, according to the entropy equation (12), $\gamma =$ constant. The radial dependence of $p_\parallel$, $p_\perp$, $|E|$ and n follow from (19), (17), (15) and (16). The ram pressure, normalized to the value of $L/\Omega_{\rm s}r^2c$ at the cut-off radius is

$$\tilde{P} = \frac{\nu_{\rm w}(R)}{\mu R^2} \ , \tag{21}$$

where $\nu_{\rm w}(R)$, which is the ratio of the momentum flux density to the particle flux density, is defined in analogy with (17) as

$$\nu_{\rm w}(R) = p_\parallel + \frac{\gamma_{\rm w}^2p_\perp^2\left(1+\beta_{\rm w}^2\right)}{2p_\parallel} \ . \tag{22}$$

For circular polarization, Eq. (20) also allows one to construct the electromagnetic Hugoniot curve found by Arka & Kirk (2012). Whereas the dispersion curves follow from the additional constraint $\gamma =$ constant, the Hugoniot curve is the locus of points under the constraint $\nu_{\rm w}(R) = \nu =$ constant. In the limit of a flow carrying zero Poynting flux, which can convert only into a wave of zero amplitude, these two curves coincide, $\gamma = \mu = \nu_{\rm w} =$ constant, and lie on the line

$$R = \gamma_{\rm w}\mu^{1/2}\left(\mu^2-1\right)^{-1/4} \ . \tag{23}$$

3.3. *Confined and freely expanding modes*

The radial evolution of $p_\perp$ and $\tilde{P}$, for $\mu = 10^4$ are shown in Fig. 1 for various values of γ, together with the Hugoniot curve for a particular choice of σ (and, hence, ν).

At large R, two modes propagate: a freely expanding mode in which the second term in (20) is negligible:

$$p_\perp \to \sqrt{\mu\left(\mu-\gamma\right)}/R \ , \tag{24}$$

$$p_\parallel \to \left(\gamma^2-1\right)^{1/2} \ , \tag{25}$$

$$\beta_{\rm w} \to 1 \ , \tag{26}$$

$$\gamma_{\rm w} \to \left(\gamma^2-1\right)^{1/4}R/\sqrt{\mu} \ , \tag{27}$$

$$\tilde{P} \to \frac{\mu-\gamma+\sqrt{\gamma^2-1}}{\mu R^2} \ , \tag{28}$$

and a confined mode in which the first term in (20) is negligible:

$$p_\perp \to \left(\gamma^2-1\right)^{1/2} \ , \tag{29}$$

$$p_\parallel \to \mu/R^2 \ , \tag{30}$$

$$\beta_{\rm w} \to \frac{\mu\left(\mu-\gamma\right)}{\left(\gamma^2-1\right)R^2} \ , \tag{31}$$

$$\gamma_{\rm w} \to 1 \ , \tag{32}$$

$$\tilde{P} \to \frac{\gamma^2-1}{2\mu^2} \ . \tag{33}$$

In the free-expansion mode, the direction of the fluid velocity aligns itself with the radial direction as the mode moves outwards. The radial fluid velocity tends to a constant value, the density and ram pressure drop as $1/R^2$, and the wave amplitude decreases as $1/R$. In the confined mode, on the other hand, the fluid velocity turns towards the transverse plane. The radial particle flow stagnates, and the ram pressure, density and wave amplitude all tend to constant values, such that the proper plasma frequency equals the pulsar rotation frequency.

In a wind-nebula system, in which the outflow is confined by the external medium in a slowly expanding bubble, the wind must terminate by decelerating to nonrelativistic speed at a point where its ram pressure roughly equals the external pressure. This is achieved at a shock discontinuity in an MHD picture. From Fig. 1 and Eq. (33), we see that the same effect is produced if the

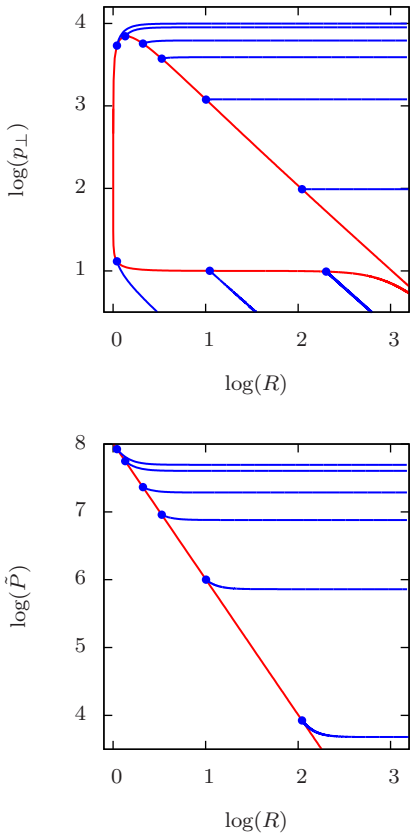

Figure 1. The electromagnetic Hugoniot curve (red) for $\mu = 10^4$, $\sigma = 100$ and the radially propagating wave modes (blue) for circularly polarized nonlinear waves launched at the blue dots. Top panel: $p_\perp$ (lower branch: free-escape mode; higher branch: confined mode). Bottom panel: the ram pressure $\tilde{P}$, defined in Eq. (21) for the confined mode only.

flow converts into a confined superluminal mode, which then decelerates at almost constant ram pressure. If this mode remained stable, it could in principle accumulate and fill a large volume around the conversion point, which would be seen as a pulsar wind nebula, as originally suggested by Rees (1971). The location of the conversion point is determined by the external pressure: the higher the surrounding pressure, the closer it lies to the pulsar. As can be seen from Fig. 2, the ram pressure changes by less than a factor of 2 between the conversion point and $R \to \infty$. Consequently, this point is located at roughly the position expected for the termination shock in the MHD picture.

3.4. *Zones of stability*

However, as discussed above, once the mode has slowed down sufficiently, it is subject to strong parametric instabilities, which ultimately dissipate the coherent oscillation, leaving behind the relativistic electron positron plasma and residual magnetic field that fill the pulsar wind nebula. In analogy with the MHD picture, we refer to the point at which instabilities arise in this scenario as the "termination shock". The region between the point at which the confined mode is launched and the termination shock is then an extended "precursor".

The propagation and stability properties of the precursor are completely determined by equations (20) and (1)

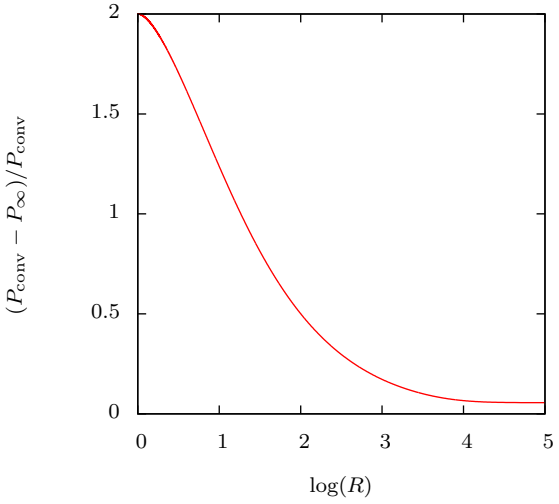

Figure 2. The fractional difference between the ram pressure $P_{\rm conv}$ at the conversion point and its value P_∞ at $R \to \infty$, plotted for the confined mode with $\mu = 10^4$ and $\sigma = 100$.

and can be extracted analytically and plotted relatively straightforwardly. In pulsars, we are concerned with relativistic flows of low mass-loading, $\mu \gg 1$, which can be assumed to be supersonic $\sigma \lesssim \mu^{2/3}$. Therefore, we present here only simplified expressions obtained to lowest order in an expansion in powers of $\epsilon \sim \mu^{-1/3} \sim \sigma^{-1/2}$. In this approximation, the stability criterion (1) for a stationary wave mode ($\beta_{\rm w} = 0$) is

$$S \approx \mu^2 \left(R^2 - 2\sqrt{R^4 - 1} \right) / R^2 \; > \; 0 \; . \qquad (34)$$

Thus, stationary modes, for which the H-frame coincides with the laboratory frame, are stable only close to the cut-off radius, in the range $1 < R < (4/3)^{1/4}$. This region is illustrated in Fig. 3. In fact, the region of stability extends also to modes which are not stationary in the lab. frame. As is clear from the definition of S in Eq. (1), the waves are formally stable along the limiting line for weak waves (23), on which $p_\perp = 0$. But the region of stability reduces to a thin layer in the neighborhood of this line as R increases. Assuming $\gamma_{\rm w} \sim R \gtrsim \sqrt{\sigma}$, we find approximate roots of S at

$$R = \gamma_{\rm w}(8 \pm 4\sqrt{3}) \; . \qquad (35)$$

Thus, at large $\gamma_{\rm w}$, the zone of stability lies in the range $\gamma_{\rm w} < R < 1.07\gamma_{\rm w}$.

Equation (35) reveals a second stable region, which, for large $\gamma_{\rm w}$, lies at $R > 14.9\gamma_{\rm w}$. This region is illustrated in Fig. 4. For $R \sim \sigma$, it is bounded from below by the line $\gamma_{\rm w} = 2$, but this boundary drops to lower wave group speeds at larger R. The stable zone vanishes inside a critical radius, which is roughly where the line $\gamma_{\rm w} = 2$ intersects the line $R = \gamma_{\rm w}\left(8 + 4\sqrt{3}\right)$, at $R = 30$.

The Hugoniot curves for $\sigma = 100$ are also shown in Figs. 3 and 4. Expanding the expression for the confined mode branch to lowest order in $\epsilon \sim \mu^{-1/3} \sim \sigma^{-1/2}$, and combining this with the approximate expression for the lower bound of the stability curve (see Appendix D) shows that the launched waves are stable, provided the

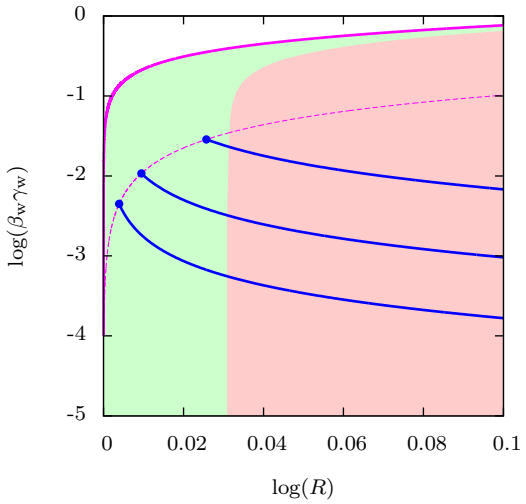

Figure 3. The inner zone of stability. Electromagnetic Hugoniot curves are plotted showing the group four-speed ($\beta_{\rm w}\gamma_{\rm w}$) as a function of radius R for $\mu = 10^4$, $\sigma = 100$ (red lines, solid: free expansion branch, dashed: confined branch). In blue, the radial evolution of three confined modes launched at different radii are plotted. In the green region the waves are stable according to the criterion given in Eq. (1). In the pink shaded region they are unstable. The unshaded region depicts waves with inwardly directed Poynting flux which are not relevant to pulsar winds.

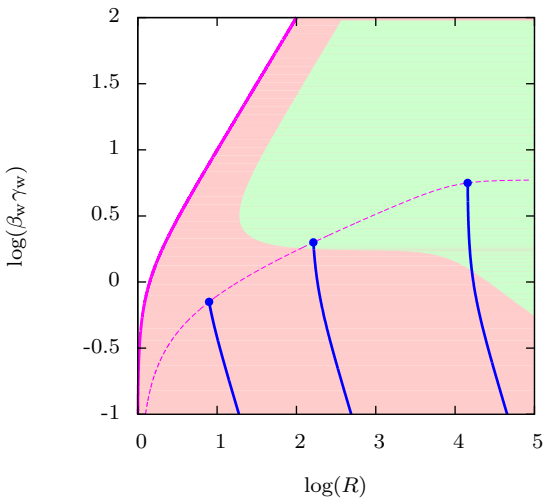

Figure 4. The outer zone of stability. The same Hugoniot curves are plotted as in Fig. 3, together with three confined modes, launched at larger radius. The pink and green shadings again depict unstable and stable regions, respectively. The inner zone of stability lies close to the Hugoniot curve of the free escape mode, and is not visible on the scale of this figure.

launching radius exceeds a critical value

$$R > R_{\rm crit} \approx 100 \ . \tag{36}$$

The length of a precursor consisting of a stable, nonlinear electromagnetic wave can be estimated from Figs 3 and 4. In the inner stable region, the slowing down of the wave plays a relatively minor role. Even at constant group speed, the precursor wave enters the unstable zone after propagating for at most 4% of the radius. Depending on the pulsar parameters, which fix the relationship of the dimensionless scaled radius R to the light-cylinder radius, the stable precursor can nevertheless extend over many wavelengths. In the outer stable region, however, it is the wave deceleration that drives the precursor wave into the unstable region. The extent in radius over which this occurs can be estimated as $\Delta R/R \approx {\rm d}\log R/{\rm d}\log(\beta_{\rm w}\gamma_{\rm w})$. Using Eq. (20), we find for the confined mode $\Delta R/R \approx 1/8$, so that here again, the precursor extends over a relatively small fraction ($\sim 10\%$) of the radius, which may, however, correspond to many wavelengths.

4. DISCUSSION

The effects of spherical geometry on strong, radially propagating electromagnetic modes are potentially important for the structure of pulsar winds and their termination shocks. However, previous work on this topic (Asseo et al. 1984; Kirk 2010), is flawed because it assumes the divergence of the radial momentum flux vanishes. In fact, as we show above and in Appendix B, the radial momentum equation does not yield a conservation equation; as the modes propagate, the transverse and parallel degrees of freedom exchange energy with each other, keeping the total energy is conserved. We show that, for arbitrary polarization, there exists an additional conserved quantity — the phase-averaged Lorentz factor of the particles $\langle\gamma\rangle$ — which, together with the conservation of energy and particle fluxes, enables the system to be integrated.

Nevertheless, the case of general polarization remains unwieldy, so that the discussion we present of the mode properties is mainly restricted to circularly polarized modes, for which phase-averages can be dropped. The dispersion curves, which we here call electromagnetic Hugoniot curves, were found by Arka & Kirk (2012) for linearly polarized modes with vanishing phase-averaged magnetic field. They closely resemble those for circular polarization, suggesting that this simplification is not an important restriction, at least in the region close to the equatorial plane.

The electromagnetic Hugoniot curve admits two solutions for radial propagation (Arka & Kirk 2012). By examining the asymptotic behavior of waves launched on these branches, we identify them as a free-escape and a confined mode, with very different properties. The group speed of the former accelerates, whereas that of the latter decelerates during outward propagation from the launching point. We argue that, in outflows such as those from pulsars surrounded by nebulae, only the confined mode can provide a self-consistent solution matching a relativistic, highly magnetized wind to a slowly expanding, weakly magnetized nebula. We show that the external pressure determines the radius at which a confined mode must be launched in order to realize such a solution. The higher the pressure, the closer to the star the launching, or conversion, takes place. However, we do not discuss the physical mechanism by which the wind converts from one mode to the other. This question demands a different approach, and most likely necessitates either two-fluid or particle-in-cell simulations. It has been addressed recently (Amano & Kirk 2013), but only for a very limited range of physical parameters, corresponding to a launching radius close to the critical radius $r_{\rm c}$.

A confined mode becomes unstable against longitudinal density perturbations when the particle stream-

Table 1
Pulsar wind nebulae studied by Bucciantini et al. (2011).

	Crab	3C 58	B1509-58	Kes75	W44	K2/K3 Kookaburra
References	1	2, 3	4,5	6	7, 8	9
$P_{\rm pulsar}$ (ms)	33	65	150	324.8	267	68.2
$L(\times 10^{38}$ erg s$^{-1})$	5	0.27	0.18	0.083	0.0043	0.1
$a_{\rm L}(\times 10^{10})$	7.6	1.8	1.4	0.98	0.22	1.1
κ (lower limit)	10^6	5×10^5	3×10^5	10^5	10^5	10^5
μ (upper limit)	1.9×10^4	8.8×10^3	1.2×10^4	2.4×10^4	5.5×10^3	2.7×10^4
$P_{\rm conv}$ (dyn cm^{-2})	$\sim10^{-8}$	3.2×10^{-10}	$\sim10^{-10}$	$\sim10^{-11}$	$>5.7\times10^{-10}$	4×10^{-10}
Conversion radius $R_{\rm conv}$ (upper limit)	575	781	800	2300	86	1979

References. — (1) Kennel & Coroniti 1984a; (2) Murray et al. 2002; (3) Slane et al. 2002; (4) Gaensler et al. 1999; (5) Yatsu et al. 2009; (6) Ng et al. 2008; (7) Frail et al. 1996; (8) Cox et al. 1999; (9) Ng et al. 2005

ing through the wave drops below a critical value. For plane, circularly polarized waves, we adopt a simple stability condition (1) against long-wavelength, parallel fluctuations proposed by Lee & Lerche (1978). In fact, obliquely propagating fluctuations may change this simple condition if they turn out to be more unstable than the parallel ones (Lee & Lerche 1978), but we are not aware of a suitable alternative criterion. On the other hand, waves which have a nonvanishing component of the transverse magnetic field, i.e., those which are launched at higher latitudes in pulsar winds, may be stabilized by the presence of this field (Asseo et al. 1980).

Using this criterion, we find two regions in which confined modes are stable when launched, although they subsequently propagate into an unstable region. In terms of the normalized radius, these are an outer zone, $R \gtrsim 100$, and an inner zone $R \approx 1$. These zones and the location of their boundaries are essentially independent of the parameters μ and σ of the pulsar wind, provided it is relativistic, $\mu \gg 1$, and supermagnetosonic, $\sigma < \mu^{2/3}$. However, their relevance depends on where the pressure confining a particular pulsar wind places the launching point. This, in turn, depends on the radius normalization, which varies from pulsar to pulsar. In terms of the light-cylinder radius $r_{\rm L}$, the normalized radius is $R = (r/r_{\rm L})(\mu/a_{\rm L} \approx r_{\rm L}/r_{\rm c})$, where the strength parameter at the light cylinder $a_{\rm L}$ is a dimensionless measure of the spin-down power per unit solid angle: $a_{\rm L} = 3.4\times10^{10}\left[\left(L/10^{38}{\rm erg\,s^{-1}}\right)(4\pi/\Omega_{\rm s})\right]^{1/2}$.

We show in Fig. 2 that the pressure at the conversion point lies close to $L/\Omega_{\rm s} r^2 c$, which can be written as

$$P_{\rm conv} = \frac{10^{-6}}{R^2}\left(\frac{\mu}{10^4}\right)^2\left(\frac{P_{\rm pulsar}}{1\,{\rm second}}\right)^{-2}\ {\rm dyn\,cm^{-2}}\ , \quad (37)$$

where $P_{\rm pulsar}$ is the rotation period of the pulsar. This must be compared with the nebular pressure, usually estimated from the volume-averaged, equipartition magnetic and particle energy densities required to produce the nebular synchrotron emission (Kennel & Coroniti 1984a). These estimates, together with the implied normalized radius of the conversion point $R_{\rm conv}$ are listed in Table 1 for those pulsar wind nebulae studied by Bucciantini et al. (2011). We see from this table that the isolated pulsars can be expected to launch stable precursor waves at the termination shock, since in all but one case $R_{\rm conv} > 100$. The only exception is the pulsar in the supernova remnant W44, which, however, is known to be interacting with a dense molecular cloud (Cox et al. 1999).

The PWNe of isolated pulsars in starburst galaxies have recently been proposed as sources of the very high energy emission from those galaxies (Mannheim et al. 2012; Ohm & Hinton 2013). The pressure in the interstellar medium in these objects ($\sim 10^{-9}\,{\rm dyn\,cm^{-2}}$) is some three orders of magnitude greater than in the Milky Way. If this scaling is reflected in the pressure in PWN bubbles, the estimated conversion radii fall by a factor of 30. From Table 1, we see that the precursor waves would in this case be launched in the unstable zone $R < 100$. It seems reasonable to suppose that the shock structure will be strongly influenced by such a change. However, the possible implications for particle acceleration and the resulting non-thermal photon emission remain unknown.

The inner zone of stability, on the other hand, may be of importance for pulsar winds in high pressure environments, such as outflows from a companion star. Several gamma-ray binaries are likely to fall into this class (Dubus 2006) but so far only one of them, B1259−63, harbors a pulsar with a measured period. Its spin-down power $L = 8\times10^{35}\,{\rm erg\,s^{-1}}$, implies $a_{\rm L} = 3\times10^9$, an order of magnitude lower than that of the Crab. Assuming young and middle-aged pulsars have a pair multiplicity $\kappa = a_{\rm L}/(4\mu)$ that is at least 10^5 (Bucciantini et al. 2011), we find, for B1259−63, $\mu \gtrsim 7.6\times10^3$. The confining pressure at periastron, and, hence the pressure at the conversion point, can be estimated as $P_{\rm conv} \geq 2.5\times10^{-4}\,{\rm dyn\,cm^{-2}}$ (Dubus 2006). This implies $R_{\rm conv} \approx 1$, i.e., the conversion point lies roughly at the critical radius inside which superluminal waves cannot propagate. Since the confining pressure varies over the binary orbit, it appears possible that the pulsar wind in this object will terminate at $r < r_{\rm c}$ close to periastron, but at $r > r_{\rm c}$ at larger binary separations. At the transition points, the conversion point passes through the inner stable zone, and, according to Fig 3, a stable precursor wave is possible for a brief interval of phase.

5. CONCLUSIONS

Our main results are the derivation for strong superluminal waves of an analogue of the hydrodynamical entropy equation, the demonstration that two kinds of wave, confined and freely expanding, propagate in spherical geometry, and the identification of two zones of stabil-

ity of the confined mode in pulsar winds. Strictly speaking, the latter two results apply only to circularly polarized modes, but the similarity of the dispersion curves for linear and circular modes suggest this is not a serious restriction.

The application of these results to PWN around isolated pulsars and around pulsars in gamma-ray binaries suggests different termination shock structures depending on the confining pressure. However, the implications for particle acceleration and, hence possible observational signatures remain a topic for future work.

We thank Ioanna Arka, Jérôme Pétri and Takanobu Amano for fruitful discussions.

APPENDIX

A. RADIAL PROPAGATION OF LARGE-AMPLITUDE WAVES

To solve a coupled system of two-fluid and Maxwell equations in spherical geometry, we use a standard perturbation technique, following Asseo et al. (1984) and Kirk & Mochol (2011a,b). We assume two timescales, on which the wave properties change: a fast scale – determined by the pulsar rotation period, and a slow scale, on which the wave quantities evolve slowly due to spherical expansion. The "fast" variable is the WKB-like phase of a wave

$$\phi = \omega\left(t - \int^r \frac{dr'}{c\beta(r')}\right) \ , \tag{A1}$$

where $\beta = 1/\beta_{\rm w}$ is the superluminal phase velocity of a wave, $\beta_{\rm w}$ is the subluminal group speed. The "slow" radial coordinate is defined by the light cylinder distance $r_{\rm L}$ as

$$\rho = \epsilon\frac{r}{r_{\rm L}} \ , \tag{A2}$$

where $\rho \sim 1$ and $\epsilon \sim r_{\rm L}/r \ll 1$ is a small parameter. The time and space derivatives, expressed in terms of the new variables ϕ and ρ, take the following form:

$$\frac{\partial}{\partial t} \to \omega\frac{\partial}{\partial\phi} \ , \ \frac{\partial}{\partial r} \to \epsilon\frac{\omega}{c}\frac{\partial}{\partial\rho} - \frac{\omega\beta_{\rm w}}{c}\frac{\partial}{\partial\phi} \ , \ \gamma\frac{d}{dt} \to \epsilon\frac{\omega}{c}p_\parallel\frac{\partial}{\partial\rho} + \omega\Delta\frac{\partial}{\partial\phi} \ , \tag{A3}$$

where $\Delta = \gamma - \beta_{\rm w}p_\parallel$. Expressions (A3) are substituted into the equations that govern wave propagation (e.g., Clemmow 1974b; Kennel & Pellat 1976), and, in addition, all the dependent variables in these equations are expanded in ϵ to the first order, i.e., $\gamma = \gamma^{(0)} + \epsilon\gamma^{(1)}$ etc. The proper density of each plasma species and the electromagnetic fields are expressed in a dimensionless form: $n \to nm\omega^2/8\pi e^2$, $E \to eE/mc\omega$, $B \to eB/mc\omega$, where $E = E_y + iE_z$ and $B = B_y + iB_z$ are complex quantities (so are the transverse momenta $p_\perp = p_y + ip_z$).

In the lowest order in ϵ we obtain the equations describing plane waves. Those are the continuity equation:

$$\frac{\partial}{\partial\phi}\left(n^{(0)}\Delta^{(0)}\right) = 0 \ , \tag{A4}$$

Faraday's and Ampère's laws:

$$\beta_{\rm w}\frac{\partial E^{(0)}}{\partial\phi} + i\frac{\partial B^{(0)}}{\partial\phi} = 0 \ , \tag{A5}$$

$$-\beta_{\rm w}\frac{\partial B^{(0)}}{\partial\phi} + i\frac{\partial E^{(0)}}{\partial\phi} + in^{(0)}p_\perp^{(0)} = 0 \ , \tag{A6}$$

and momentum/energy conservation multiplied by n:

$$n^{(0)}\Delta^{(0)}\frac{\partial p_\parallel^{(0)}}{\partial\phi} + n^{(0)}{\rm Im}\left(p_\perp^{(0)}B^{(0)*}\right) = 0 \ , \tag{A7}$$

$$n^{(0)}\Delta^{(0)}\frac{\partial p_\perp^{(0)}}{\partial\phi} - n^{(0)}\left(\gamma^{(0)}E^{(0)} + ip_\parallel^{(0)}B^{(0)}\right) = 0 \ , \tag{A8}$$

$$n^{(0)}\Delta^{(0)}\frac{\partial\gamma^{(0)}}{\partial\phi} - n^{(0)}{\rm Re}\left(p_\perp^{(0)}E^{(0)*}\right) = 0 \ . \tag{A9}$$

Equations (A5) and (A6) imply $B^{(0)} = i\beta_{\rm w}E^{(0)}$ and $n^{(0)}p_\perp^{(0)} = -(1-\beta_{\rm w}^2)\partial E^{(0)}/\partial\phi$. Using these relations in equations (A7) and (A9), we arrive at the result that the quantity $\delta^{(0)} = p_\parallel^{(0)} - \beta_{\rm w}\gamma^{(0)}$ is phase independent.

In the first order in ϵ the equation of continuity reads:

$$\frac{\partial}{\partial\phi}\left(n^{(0)}\Delta^{(1)} + n^{(1)}\Delta^{(0)}\right) + \frac{1}{\rho^2}\frac{\partial}{\partial\rho}\left(\rho^2 n^{(0)}p_\parallel^{(0)}\right) = 0 \ , \tag{A10}$$

Faraday's and Ampère's laws are:

$$-\beta_{\rm w}\frac{\partial E^{(1)}}{\partial\phi}-i\frac{\partial B^{(1)}}{\partial\phi}+\frac{1}{\rho}\frac{\partial}{\partial\rho}\left(\rho E^{(0)}\right)=0\ , \tag{A11}$$

$$-\beta_{\rm w}\frac{\partial B^{(1)}}{\partial\phi}+i\frac{\partial E^{(1)}}{\partial\phi}+i\left(n^{(0)}p_\perp^{(1)}+n^{(1)}p_\perp^{(0)}\right)+\frac{1}{\rho}\frac{\partial}{\partial\rho}(\rho B^{(0)})=0\ , \tag{A12}$$

and momentum/energy equations, after multiplying by n, give:

$$\left(n^{(1)}\Delta^{(0)}+n^{(0)}\Delta^{(1)}\right)\frac{\partial p_\parallel^{(0)}}{\partial\phi}+n^{(0)}\Delta^{(0)}\frac{\partial p_\parallel^{(1)}}{\partial\phi}+\left[n\,{\rm Im}\left(p_\perp B^*\right)\right]^{(1)}+n^{(0)}p_\parallel^{(0)}\frac{\partial p_\parallel^{(0)}}{\partial\rho}=n^{(0)}\frac{|p_\perp^{(0)}|^2}{\rho}\ , \tag{A13}$$

$$\left(n^{(1)}\Delta^{(0)}+n^{(0)}\Delta^{(1)}\right)\frac{\partial p_\perp^{(0)}}{\partial\phi}+n^{(0)}\Delta^{(0)}\frac{\partial p_\perp^{(1)}}{\partial\phi}-\left[n\left(\gamma E+ip_\parallel B\right)\right]^{(1)}+n^{(0)}p_\parallel^{(0)}\frac{\partial p_\perp^{(0)}}{\partial\rho}=-n^{(0)}\frac{p_\parallel^{(0)}p_\perp^{(0)}}{\rho}\ , \tag{A14}$$

$$\left(n^{(1)}\Delta^{(0)}+n^{(0)}\Delta^{(1)}\right)\frac{\partial\gamma^{(0)}}{\partial\phi}+n^{(0)}\Delta^{(0)}\frac{\partial\gamma^{(1)}}{\partial\phi}-\left[n\,{\rm Re}\left(p_\perp E^*\right)\right]^{(1)}+n^{(0)}p_\parallel^{(0)}\frac{\partial\gamma^{(0)}}{\partial\rho}=0\ . \tag{A15}$$

To ensure that the first-order quantities have regular (nonsecular) behavior, we impose the condition that they are periodic in ϕ. This suffices to determine the slow radial dependence of the lowest-order, phase-averaged terms. For example, integrating Eq. (A10) over ϕ, we obtain

$$\frac{1}{\rho^2}\frac{d}{d\rho}\left(\rho^2\left\langle n^{(0)}p_\parallel^{(0)}\right\rangle\right)=0\ . \tag{A16}$$

Next, we express the transverse momentum in terms of the fields using Faraday's and Ampère's laws, (A11) and (A12), which allows us to calculate the phase-averaged forces:

$$\left\langle\left[n\,{\rm Re}\left(p_\perp E^*\right)\right]^{(1)}\right\rangle=-\frac{1}{\rho^2}\frac{\partial}{\partial\rho}\left\langle\rho^2\beta_{\rm w}|E^{(0)}|^2\right\rangle\ , \tag{A17}$$

$$\left\langle\left[n\,{\rm Im}\left(p_\perp B^*\right)\right]^{(1)}\right\rangle=\frac{1}{2}\frac{1}{\rho^2}\frac{\partial}{\partial\rho}\left\langle\rho^2\left(1+\beta_{\rm w}^2\right)|E^{(0)}|^2\right\rangle\ . \tag{A18}$$

Substituting those into the equations of motion (A15) and (A13), we obtain the conservation of the total energy flux and evolution of the radial momentum flux, respectively:

$$\frac{1}{\rho^2}\frac{d}{d\rho}\left[\rho^2\left\langle n^{(0)}p_\parallel^{(0)}\gamma^{(0)}+\beta_{\rm w}\left|E^{(0)}\right|^2\right\rangle\right]=0\ , \tag{A19}$$

$$\frac{1}{\rho^2}\frac{d}{d\rho}\left[\rho^2\left\langle n^{(0)}{p_\parallel^{(0)}}^2+\frac{1}{2}\left(1+\beta_{\rm w}^2\right)\left|E^{(0)}\right|^2\right\rangle\right]=\frac{1}{\rho}\left\langle n^{(0)}{p_\perp^{(0)}}^2\right\rangle\ . \tag{A20}$$

B. CONSERVATION OF $\langle\gamma\rangle$

The analogue of the hydrodynamic entropy equation is obtained by multiplying (A15) by $\beta_{\rm w}$ and subtracting it from (A13):

$$\left(n^{(1)}\Delta^{(0)}+n^{(0)}\Delta^{(1)}\right)\frac{\partial\delta^{(0)}}{\partial\phi}+n^{(0)}\Delta^{(0)}\frac{\partial\delta^{(1)}}{\partial\phi}+\beta_{\rm w}\left[n\,{\rm Re}\left(p_\perp E^*\right)\right]^{(1)}+\left[n\,{\rm Im}\left(p_\perp B^*\right)\right]^{(1)}$$
$$+n^{(0)}p_\parallel^{(0)}\frac{\partial p_\parallel^{(0)}}{\partial\rho}-\beta_{\rm w}n^{(0)}p_\parallel^{(0)}\frac{\partial\gamma^{(0)}}{\partial\rho}-n^{(0)}\frac{|p_\perp^{(0)}|^2}{\rho}=0\ . \tag{B1}$$

It is shown in Appendix A that the lowest order equations imply that $\delta^{(0)}$ is phase independent, and the first order quantities are required to be periodic in ϕ. Therefore, phase averaging of (B1) immediately cancels first two terms, and the remaining part takes the form

$$-\beta_{\rm w}\frac{1}{\rho^2}\frac{\partial}{\partial\rho}\left\langle\rho^2\beta_{\rm w}|E^{(0)}|^2\right\rangle+\frac{1}{2}\frac{1}{\rho^2}\frac{\partial}{\partial\rho}\left\langle\rho^2\left(1+\beta_{\rm w}^2\right)|E^{(0)}|^2\right\rangle$$
$$+\left\langle n^{(0)}p_\parallel^{(0)}\frac{\partial p_\parallel^{(0)}}{\partial\rho}\right\rangle-\beta_{\rm w}\left\langle n^{(0)}p_\parallel^{(0)}\frac{\partial\gamma^{(0)}}{\partial\rho}\right\rangle-\frac{1}{\rho}\left\langle n^{(0)}|p_\perp^{(0)}|^2\right\rangle=0\ , \tag{B2}$$

where we have used the expressions for phase-averaged forces (A17) and (A18). In the following we omit superscript "0" and further simplify the equation (B2) by the momentum relation $p_\parallel^2 = \gamma^2 - p_\perp^2 - 1$, so that it reads

$$\frac{\left\langle E^2 \right\rangle}{\gamma_{\rm w}^2 \rho} + \frac{1}{2\gamma_{\rm w}^2}\frac{\partial \left\langle E^2 \right\rangle}{\partial \rho} + n_0\Delta_0 \frac{\partial \left\langle \gamma \right\rangle}{\partial \rho} - \frac{1}{2}\left\langle n \frac{\partial p_\perp^2}{\partial \rho} \right\rangle - \frac{\left\langle n p_\perp^2 \right\rangle}{\rho} = 0 \ . \tag{B3}$$

The first term in (B3) cancels the last term, since:

$$\left\langle E^2 \right\rangle = \int_0^{2\pi} d\phi E^2 = \int_0^{2\pi} d\phi \frac{\partial p_\perp^*}{\partial \phi}\frac{\partial p_\perp}{\partial \phi} = -\int_0^{2\pi} d\phi p_\perp^* \frac{\partial^2 p_\perp}{\partial \phi^2} = \int_0^{2\pi} d\phi \gamma_{\rm w}^2 n p_\perp^2 = \gamma_{\rm w}^2 \left\langle n p_\perp^2 \right\rangle \ . \tag{B4}$$

Here in the second step we use the equation (A8) and (A5), which together imply $E^{(0)} = \partial p_\perp^{(0)}/\partial\phi$, and we integrate once by parts. Further simplification follows from Eq. (A6): $\partial^2 p_\perp/\partial\phi^2 = \partial E^{(0)}/\partial\phi = -\gamma_{\rm w}^2 n p_\perp$. The same relations prove that the second term in the entropy equation (B3) cancels the fourth term:

$$\begin{aligned}\left\langle n \frac{\partial p_\perp^2}{\partial \rho} \right\rangle = \int_0^{2\pi} d\phi \left(n p_\perp \frac{\partial p_\perp^*}{\partial \rho} + n p_\perp^* \frac{\partial p_\perp}{\partial \rho} \right) &= -\frac{1}{\gamma_{\rm w}^2}\int_0^{2\pi} d\phi \left(\frac{\partial E}{\partial \phi}\frac{\partial p_\perp^*}{\partial \rho} + \frac{\partial E^*}{\partial \phi}\frac{\partial p_\perp}{\partial \rho} \right) \\ &= \frac{1}{\gamma_{\rm w}^2}\int_0^{2\pi} d\phi \left(E\frac{\partial E^*}{\partial \rho} + E^*\frac{\partial E}{\partial \rho} \right) = \frac{1}{\gamma_{\rm w}^2}\frac{\partial}{\partial \rho}\left\langle E^2 \right\rangle \ . \end{aligned} \tag{B5}$$

Thus, Eq. (B3) implies that independently of the wave polarization the phase-averaged Lorentz factor of the particles stays constant during the radial expansion:

$$\frac{\partial \left\langle \gamma \right\rangle}{\partial \rho} = 0 \ . \tag{B6}$$

C. LINEAR POLARIZATION

For linearly polarized waves all the quantities are phase dependent. It is convenient to use the phase variable $y = E/E_0$, chosen to be $y = 1$ for the phase ϕ, for which the electric field takes the maximum value E_0. The nonlinear dispersion relation follows from the periodicity requirement

$$1 = \frac{2}{\pi}\int_0^1 \frac{dy}{|dy/d\phi|} \ , \tag{C1}$$

and Ampère's law takes the form

$$\frac{dy}{d\phi} = -\frac{\omega_{\rm p}^2 \gamma_{\rm w}^2 p_\perp}{E_0 \omega^2} = -\frac{\Delta_0 \omega_{\rm p0}^2 \gamma_{\rm w}^2}{E_0 \omega^2}\frac{p_\perp}{\Delta} \ , \tag{C2}$$

where $\omega_{\rm p0}^2 = 8\pi e^2 n_0/m$, and the continuity equation (A4) implies that $n\Delta \equiv n_0\Delta_0$ is phase-independent. In radial evolution equations all the phase averages have to be calculated explicitly, i.e.,

$$\left\langle X \right\rangle = \frac{2}{\pi}\int_0^1 X(y)\frac{dy}{|dy/d\phi|} \ . \tag{C3}$$

Dependence of plane-wave particle momenta γ, $p_\perp$, $p_\parallel$ on y one obtains by integrating equations of motion, e.g., Kennel & Pellat (1976):

$$\gamma = \gamma_0 + \frac{\omega^2 E_0^2}{2\omega_{\rm p0}^2 \Delta_0 \gamma_{\rm w}^2}(1 - y^2) \ , \tag{C4}$$

$$p_\parallel = p_{\parallel 0} + \frac{\omega^2 E_0^2 \beta_{\rm w}}{2\omega_{\rm p0}^2 \Delta_0 \gamma_{\rm w}^2}(1 - y^2) \ , \tag{C5}$$

$$p_\perp = (\gamma^2 - p_\parallel^2 - 1)^{1/2} \ , \tag{C6}$$

where $\gamma_0^2 = p_{\parallel 0}^2 + 1$. The set of equations which describes radial propagation of a linearly polarized wave with variables n_0, $p_{\parallel 0}$, E_0, $p_\perp$, γ_0, $\beta_{\rm w}$ is given by equations (8), (9), and (12), in which the phase averages have to be calculated explicitly according to Eq. (C3), together with (C1) and (C6).

D. THE OUTER STABILITY ZONE

The Hugoniot curves are determined by Eqs. (17) and (22), where $\nu_{\rm w}(R) = \nu$ is a constant, related to μ and σ by (4). These equations are complemented by (19) and momentum relation $\gamma = (1 + p_\perp^2 + p_\parallel^2)^{1/2}$. Finding $p_\perp$ from (22)

and substituting to (17), we obtain a biquadratic equation for radius R as a function of the wave Lorentz factor $\gamma_{\rm w}$. For the confined mode branch the larger root is relevant. The largest term in the expansion in $\epsilon \sim \mu^{-1/3} \sim \sigma^{-1/2}$ reads:

$$R^2 \approx \frac{\gamma_{\rm w}^2 - 2\gamma_{\rm w}^2\left(2\gamma_{\rm w}^2-1\right)\left(\gamma_{\rm w}^2-1\right)^{1/2}\left[2\gamma_{\rm w}\left(\gamma_{\rm w}-\sqrt{\gamma_{\rm w}^2-1}\right)-1\right]^{1/2} - 2\gamma_{\rm w}^3\left(2\gamma_{\rm w}^2-1\right)\left(\gamma_{\rm w}-\sqrt{\gamma_{\rm w}^2-1}\right)}{4\gamma_{\rm w}\left(2\gamma_{\rm w}-\sqrt{\gamma_{\rm w}^2-1}\right)-8\gamma_{\rm w}^3\left(\gamma_{\rm w}-\sqrt{\gamma_{\rm w}^2-1}\right)-1} \ . \quad \text{(D1)}$$

The lower bound on $\gamma_{\rm w}$, and thus R, for which the Hugoniot curve implies stable initial conditions for a wave at launch, is obtained from the stability condition (1), in which the particle momenta are transformed from the H-frame to the lab frame: $\gamma' = \gamma_{\rm w}(\gamma - \beta_{\rm w} p_\parallel)$, $p'_\parallel = \gamma_{\rm w}(p_\parallel - \beta_{\rm w}\gamma)$. Expanding in $\epsilon \sim \mu^{-1/3} \sim \sigma^{-1/2}$, and assuming for large radii $R \sim \epsilon^{-1}$, in the lowest order Eq. (1) takes the form

$$\frac{2\left(-2\gamma_{\rm w}^3+\gamma_{\rm w}^4\right)}{\left(-1+2\gamma_{\rm w}^2\right)} \gtrsim 0 \ . \quad \text{(D2)}$$

This implies the lower bound $\gamma_{\rm w} \approx 2$, and thus Eq. (D1) implies the relation (36).

REFERENCES

Amano, T., & Kirk, J. G. 2013, submitted to ApJ
Arka, I., & Kirk, J. G. 2012, ApJ, 745, 108, 1109.2756
Asseo, E., Kennel, F. C., & Pellat, R. 1975, A&A, 44, 31
Asseo, E., Llobet, X., & Schmidt, G. 1980, Phys. Rev. A, 22, 1293
Asseo, E., Pellat, R., & Llobet, X. 1984, A&A, 139, 417
Begelman, M. C. 1998, ApJ, 493, 291, arXiv:astro-ph/9708142
Bucciantini, N., Arons, J., & Amato, E. 2011, MNRAS, 410, 381
Clemmow, P. C. 1974a, Journal of Plasma Physics, 12, 297
——. 1974b, Journal of Plasma Physics, 12, 297
——. 1977, Journal of Plasma Physics, 17, 301
Cox, D. P., Shelton, R. L., Maciejewski, W., Smith, R. K., Plewa, T., Pawl, A., & Różyczka, M. 1999, ApJ, 524, 179
Drake, J. F., Kaw, P. K., Lee, Y. C., Schmid, G., Liu, C. S., & Rosenbluth, M. N. 1974, Physics of Fluids, 17, 778
Dubus, G. 2006, A&A, 456, 801, arXiv:astro-ph/0605287
Frail, D. A., Giacani, E. B., Goss, W. M., & Dubner, G. 1996, ApJ, 464, L165, arXiv:astro-ph/9604121
Gaensler, B. M., Brazier, K. T. S., Manchester, R. N., Johnston, S., & Green, A. J. 1999, MNRAS, 305, 724, arXiv:astro-ph/9901262
Kennel, C. F., & Coroniti, F. V. 1984a, ApJ, 283, 694
——. 1984b, ApJ, 283, 710
Kennel, C. F., & Pellat, R. 1976, Journal of Plasma Physics, 15, 335
Kirk, J. G. 2010, Plasma Physics and Controlled Fusion, 52, 124029, 1008.0536
Kirk, J. G., Lyubarsky, Y., & Petri, J. 2009, in Astrophysics and Space Science Library, Vol. 357, Astrophysics and Space Science Library, ed. W. Becker, 421, arXiv:astro-ph/0703116
Kirk, J. G., & Mochol, I. 2011a, ApJ, 729, 104, 1012.0307
——. 2011b, ApJ, 736, 165
Kirk, J. G., & Skjæraasen, O. 2003, ApJ, 591, 366, arXiv:astro-ph/0303194
Lee, M. A., & Lerche, I. 1978, Journal of Plasma Physics, 20, 313
——. 1980, Journal of Plasma Physics, 24, 89
Lyubarsky, Y. 2010, ApJ, 725, L234, 1012.1411
Lyubarsky, Y., & Kirk, J. G. 2001, ApJ, 547, 437, arXiv:astro-ph/0009270
Lyubarsky, Y., & Liverts, M. 2008, ApJ, 682, 1436, 0805.0085
Lyubarsky, Y. E. 2003, MNRAS, 345, 153, arXiv:astro-ph/0306435
Mannheim, K., Elsässer, D., & Tibolla, O. 2012, Astroparticle Physics, 35, 797, 1010.2185
Max, C., & Perkins, F. 1972, Physical Review Letters, 29, 1731
Max, C. E. 1973, Physics of Fluids, 16, 1480
Melatos, A., & Melrose, D. B. 1996, MNRAS, 279, 1168
Murray, S. S., Slane, P. O., Seward, F. D., Ransom, S. M., & Gaensler, B. M. 2002, ApJ, 568, 226, arXiv:astro-ph/0108489
Ng, C.-Y., Roberts, M. S. E., & Romani, R. W. 2005, ApJ, 627, 904, arXiv:astro-ph/0503684
Ng, C.-Y., Slane, P. O., Gaensler, B. M., & Hughes, J. P. 2008, ApJ, 686, 508, 0804.3384
Ohm, S., & Hinton, J. A. 2013, MNRAS, 429, L70, 1210.8370
Pétri, J., & Lyubarsky, Y. 2007, A&A, 473, 683
Porth, O., Komissarov, S. S., & Keppens, R. 2012, ArXiv e-prints, 1212.1382
Rees, M. J. 1971, in IAU Symposium, Vol. 46, The Crab Nebula, ed. R. D. Davies & F. Graham-Smith, 407
Rees, M. J., & Gunn, J. E. 1974, MNRAS, 167, 1
Romeiras, F. J. 1978, Journal of Plasma Physics, 20, 479
Sironi, L., & Spitkovsky, A. 2011, ApJ, 741, 39, 1107.0977
Skjæraasen, O., Melatos, A., & Spitkovsky, A. 2005, ApJ, 634, 542, arXiv:astro-ph/0508192
Slane, P. O., Helfand, D. J., & Murray, S. S. 2002, ApJ, 571, L45, arXiv:astro-ph/0204151
Yatsu, Y., Kawai, N., Shibata, S., & Brinkmann, W. 2009, PASJ, 61, 129, 0808.0581